Desalination and Water Treatment
www.deswater.com

doi: 10.1080/19443994.2016.1206091

57 (2016) 28160–28175
December

Taylor & Francis
Taylor & Francis Group

CCD Series no-24: closed circuit desalination compared with plug flow desalination processes of partial concentrate recycling in identical four-element modules

Avi Efraty

Desalitech Ltd, P.O. Box 132, Har Adar 90836, Israel, Tel. +972 52 4765 687; Fax: +972 2 570 0262; email: avi@desalitech.com

Received 25 January 2016; Accepted 22 June 2016

ABSTRACT

In light of the growing emphasis of the desalination industry on high recovery low energy processes to save water and energy with reduced needs for handling of brine effluents, the present study evaluates the prospects of reaching such objectives with plug flow desalination (PFD) techniques of internal/external partial concentrate recycling (PCR) and closed circuit desalination (CCD) of complete concentrate recycling. Comparison between the cited RO techniques is demonstrated by means of a versatile theoretical model database which addresses the unit configuration, module design, elements' specifications, module recovery, degree of PCR, flow rates, and other pertinent parameters which contribute to trustworthy model results. A comprehensive comparative model analysis of CCD and PFD–PCR with identical four-element modules under the same module recovery, concentration polarization, and initial flow rate conditions revealed that CCD is by far the best process to achieve high recovery with exceptionally low energy not possible by any conventional PFD method including such with either internal or external PCR. While PFD with internal PCR gave permeates of somewhat better quality compared with CCD, increased recovery with PCR by this technique is limited and proceeds with a much greater energy demand. While PFD with external PCR allows increased recovery comparable to that of CCD, this is achieved at the expense of inferior quality permeates and exceptionally high energy consumption. Trends revealed in the present study for four-element modules are of general implications for CCD and for single-stage or multi-stage PFD, with/without PCR, systems of different module designs and operational conditions. The high recovery low energy prospects created by CCD, unmatched by conventional PFD techniques, have been confirmed experimentally by the reported 96% (0.34 kWh/m^3) desalination of domestic water supplies (553 μS/cm) in Kansas City, USA.

Keywords: Closed circuit desalination; CCD; Plug flow desalination (PFD); Partial concentrate recycling (PCR); PFD with PCR

1. Introduction

Conventional reverse osmosis desalination generally refers to plug flow desalination (PFD) where pressurized feed flow (Q_f) at inlet to pressure vessels (PV) splits at their outlets into two streams, one of pressurized brine (Q_b) and the other of non-pressurized permeate (Q_p) with flow balance expressed by (1) and recovery by (2). PFD can be carried out also with

internal or external partial concentrate recycling (PCR) techniques [1] of unchanged flow balance according to (1). Internal PFD–PCR takes place when part of the pressurized concentrate from modules outlets is recycled to their inlets with unchanged module recovery (MR) thereby, enable increased flux, permeate production, and system recovery (R) with increased pressure while Q_f remains unchanged. External PFD–PCR takes place by recycling some of the depressurized brine effluent to the inlet of the high pressure pump (HP) where it is mixed with fresh feed and this procedure affects increased R if flow rate of HP (Q_{HP}) and MR remain unchanged since $Q_{HP} > Q_p$. In contrast with PFD–PCR techniques, complete concentrate recycling takes place by the newly emerging closed circuit desalination (CCD) technologies for seawater [2–12] and brackish water [13–23] which are consecutive sequential batch desalination processes operated under fixed flow and variable pressure conditions. CCD processes are characterized by high recovery independent of the number of elements per module restricted only by the constituents of the feed source, low energy consumption of near absolute energy conversion efficiency without need of energy recovery devices (ERD), reduced scaling and fouling propensity, and exceptionally high operational flexibility—features unattainable by conventional PFD techniques including such with PCR. Control of CCD processes takes place by three principle selected set-points of operation independent of each other including flux (or by Q_{HP} instead), module recovery (MR) (or by cross-flow (Q_{CP}) by the circulation pump (CP) instead), and system recovery (R) (or by maximum applied pressure, or by maximum electric conductivity of recycled concentrate instead) which allow an infinite number of combinations to optimize the operation of such processes. The aforementioned CCD characteristics already meet the future goals [24] of the desalination industry for processes of higher recovery and lower energy to save water and energy and reduce the handling needs of brine effluents.

The front four elements in modules used by conventional PFD techniques are responsible for most of the permeate production and the lined elements thereafter experience a declined cross-flow of increased fouling and scaling propensity, and this has suggested the preferred four-element module configuration (ME4) for CCD apparatus, although modules of different configurations (e.g. ME, ME2, ME3, ME5, and ME6) may apply as well in the design without compromising on the high recovery and low energy feature of this technology. In light of the aforementioned, and since most of the reported CCD studies relate to systems comprising ME4 modules, the present study explores the performance characteristics of such modules in a comparative theoretical model study aimed to assess CCD and PFD–PCR.

2. A comparative model for CCD and PFD–PCR performance evaluation

The general model for CCD and PFD–PCR performance evaluation assumed identical modules, unchanged MR, and same initial flow rates of permeate, module inlet and module outlet. Identical modules and fixed MR imply conditions of unchanged average element recovery and average concentration polarization, irrespective of the process type. A theoretical model based on the assumed parameters should provide recovery-dependent correlations of energy and TDS of permeates for CCD where the entire concentrate is recycled and for PFD–PCR processes as a function of their percent recycled concentrate either internally or externally.

The present study focuses for simplicity and clarity on the four-element single module (ME4) designs displayed in Fig. 1(A)–(D) for continuous PFD (A), continuous PFD with external PCR (B), continuous PFD with internal PCR (C), and batch CCD with complete concentrate recycling (D). Despite the design resemblance between PFD with internal PCR (C) and CCD (D), these processes are governed by different performance principles since the former proceeds continuously with fixed flow and pressure at module inlet and a need for ERD to achieve high energy conversion efficiency; whereas, the latter proceeds batch-wise under fixed flow and variable pressure at module inlet with near absolute energy conversion efficiency without need for ERD in the absence of pressurized brine flow release which necessitates energy recovery. In contrast with the flow rate relationships of PFD and PFD–PCR expressed by (1) of defined recovery expressed by (2); such flow term relations for CCD are expressed by (3), recovery by (4), and MR by (5); wherein ΣV_p stands for the cumulative batch sequential volume of permeates, V_{CCD} for the intrinsic volume the closed circuit inside the apparatus, R_{CCD} for batch recovery, and Q_{CP} for the CCD cross-flow created by CP.

$$Q_f = Q_{HP} = Q_b + Q_p \tag{1}$$

$$R_{PFD} = Q_p/Q_f \times 100 \tag{2}$$

$$Q_f = Q_{HP} = Q_p \tag{3}$$

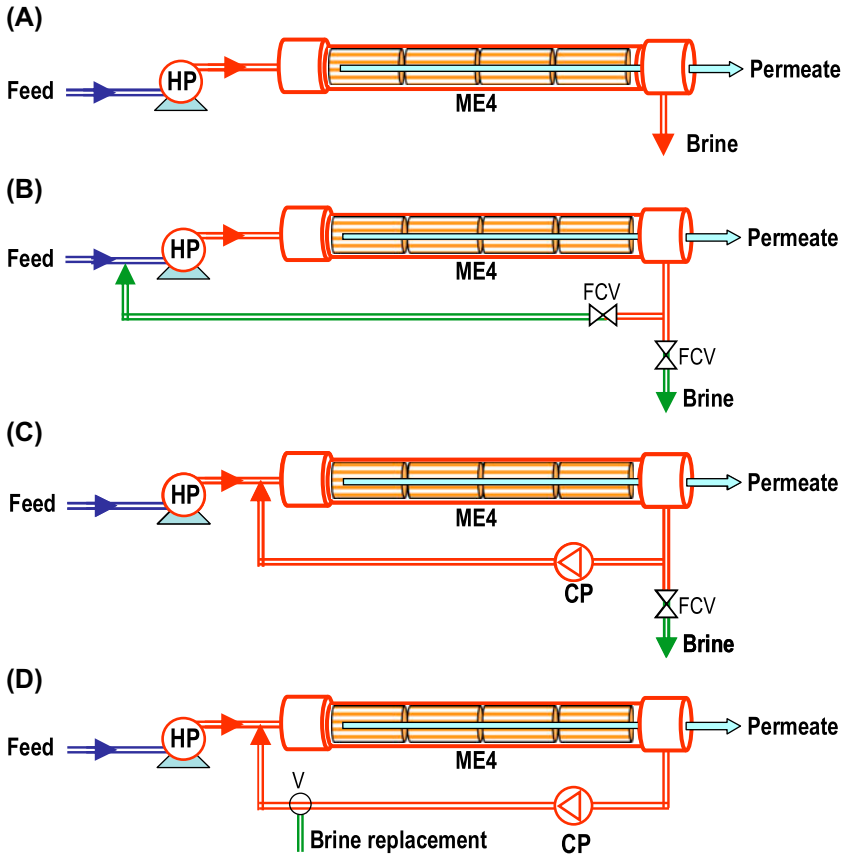

Fig. 1. Four-element single module (ME4) designs for continuous PFD (A), continuous PFD with internal PCR (B), continuous PFD with external PCR (C), and batch CCD with complete concentrate recycling (D).
Abbreviations: HP, high pressure pump; CP, circulation pump; V, valve means; FCV, flow control valve means. Colors: red for pressurized sections; Blue for non-pressurized feed lines; pale-blue for non-pressurized permeate lines; and green for non-pressurized brine lines.

$$R_{CCD} = 100 \times \Sigma V_p / (\Sigma V_p + V_{CCD}) \quad (4)$$

$$MR = 100 \times Q_p/(Q_p + Q_{CP}) = 100 \times Q_{HP}/(Q_{HP} + Q_{CP}) \quad (5)$$

3. Theoretical model database for CCD and PFD–PCR performance simulations illustrated by ME4 (E = ESPA2-MAX) apparatus at 45% MR with 0.2% NaCl feed

The comparative performance of the CCD and PFD–PCR systems is illustrated with feed of 2,000 ppm NaCl (0.20%) using the single module ME4 (E = ESPA2-MAX) apparatus of the designs displayed in Fig. 1(B) for PFD with external PCR, in Fig. 1(C) for PFD with internal PCR, and in Fig. 1(D) for batch CCD which also applies to related designs where batch performance is repeated by means of consecutive sequential techniques. The uniform performance simulation database for the processes is shown in Table 1(A)–(C) where selected parameters appear in red. The selected data pertains to the specifications of the element (ESPA2-MAX); the unit design (e.g. number of modules, elements per module, and length of PV); the CCD set-points of operation of flux and MR; and the percent increment raise of the PCR during the compared PFD processes. Other pertinent information in the database includes the source salinity and its *van't Hoff* conversion factor to osmotic pressure, the efficiency ratio of pumps, and the temperature correction factor (TCF). All other information in Table 1(A)–(C) apart from the selected parameters, originates from calculations based on common theoretical RO equations [1].

The data in Table 1(A)–(C) distinguish between CCD (Table 1(A)), PFD with internal PCR (Table 1(B)) and PFD with external PCR (Table 1(C)) of same MR (45%), average element recovery (AEC, 13.9%), and

Table 1
Theoretical model database for comparative performance of CCD (A), PFD with internal-PCR (B), and PFD with external-PCR (C) exemplified 0.2% NaCl feed using single module ME4 (E = ESPA2-MAX) apparatus operated at 45% MR with 3.26 m^3/h initial permeate production

TEST: ESPA2-MAX		UNIT DESIGN		CCD		PFD-PRC	
40.8	m2/Element	1	Modules	0.20	% NaCl	0.20	% NaCl
45.4	m3/day	4	Elements/Module	20.0	lmh - Flux	45.0	% MR
1,500	ppm NaCl	530	cm, PV length	45	% Module Recovery	5.0	% PCR
10.5	bar Applied Pressure	20	cm, PV diameter	0.58	bar Δp	7.25	m3/h - Module inlet
15	% Recovery	2	%,conduits' volume	3.26	m3/h Permeate (Q_{HP})	3.26	m3/h - Permeate (Q_p)
25	°C	15	liter per element	13.9	% av-Element Recovery	13.9	% av-Element-Recovery
99.6	% Salt Rejection	109	liter /module	1.25	av-*pf*	1.25	av-*pf*
9.3	bar NDP	109	liter/unit	3.99	m3/h CP (Q_{CP})		
46.36	l/m2/h Flux	C-->π Conversion		7.25	m3/h Module Inlet	PUMPS	
4.985	l/m2/h/bar -A	2,000	ppm NaCl	0.09	m3/cycle permeate	0.75	HP Efficiency .
0.146	l/m2/h - B	0.20	% Feed	1.63	min/cycle CCD	0.75	CP Efficiency
		1.6	bar - π			TEMPERATURE	
		8.00	π(bar)/C(%) van't-Hoff factor			25	°C
						1.00	TCF

(A) CCD SIMULATION

Module Data				Separate CCD Cycles								Combined Sequence					av-PERM	
Mode	Cycle	Inlet %	Outlet %	Time min	p_{ap} bar	av-p_{ap} bar	HP kW	CP kW	HP+CP kW	per cycle kWh/m3	PERM ppm	Time Σmin	m3 -Permeate Step	Σm3	Energy ΣkWh	REC %	SE kWh/m3	TDS ppm
CCD	0	0.20	0.200	0.00	7.1	7.1	0.86	0.09	0.95	0.290	16.4	0.0	0.000	0.000	0.0	0.0	0.290	16.4
CCD	1	0.200	0.364	1.63	7.1	7.1	0.86	0.09	0.95	0.290	16.4	1.63	0.089	0.09	0.03	45.0	0.290	16.4
CCD	2	0.290	0.527	1.63	8.4	7.8	1.01	0.09	1.10	0.337	23.8	3.27	0.089	0.18	0.06	62.1	0.314	20.1
CCD	3	0.380	0.691	1.63	9.7	8.4	1.17	0.09	1.25	0.384	31.2	4.90	0.089	0.27	0.09	71.1	0.337	23.8
CCD	4	0.470	0.855	1.63	10.9	9.0	1.32	0.09	1.41	0.431	38.6	6.53	0.089	0.36	0.13	76.6	0.361	27.5
CCD	5	0.560	1.018	1.63	12.2	9.7	1.47	0.09	1.56	0.478	45.9	8.16	0.089	0.44	0.17	80.4	0.384	31.2
CCD	6	0.650	1.182	1.63	13.5	10.3	1.63	0.09	1.71	0.525	53.3	9.80	0.089	0.53	0.22	83.1	0.408	34.9
CCD	7	0.740	1.345	1.63	14.7	10.9	1.78	0.09	1.87	0.572	60.7	11.43	0.089	0.62	0.27	85.1	0.431	38.6
CCD	8	0.830	1.509	1.63	16.0	11.6	1.93	0.09	2.02	0.619	68.1	13.06	0.089	0.7	0.32	86.7	0.455	42.2
CCD	9	0.920	1.673	1.63	17.3	12.2	2.09	0.09	2.17	0.666	75.5	14.69	0.089	0.8	0.38	88.0	0.478	45.9
CCD	10	1.010	1.836	1.63	18.5	12.8	2.24	0.09	2.33	0.713	82.9	16.33	0.089	0.9	0.45	89.1	0.502	49.6
CCD	11	1.100	2.000	1.63	19.8	13.5	2.40	0.09	2.48	0.760	90.2	17.96	0.089	1.0	0.51	90.0	0.525	53.3
CCD	12	1.190	2.164	1.63	21.1	14.1	2.55	0.09	2.63	0.807	97.6	19.59	0.089	1.1	0.58	90.8	0.549	57.0
1A	2A	3A	4A	5A	6A	7A	8A	9A	10A	11A	12A	13A	14A	15A	16A	17A	18A	19A

(B) INTERNAL PFD-PRC SIMULATION

	Module flow rates and flux									Module Concentrations			Pressures, power and energy						system
	HP	PCR		inlet	outlet	Perm.	Brine	MR	Flux	Inlet	outlet	Perm	p_{ap} (HP)	Δp(CP)	HP	CP	HP+CP	SE	REC
MODE	m3h	%	m3/h	m3/h	m3h	m3h	m3h	%	lmh	%	%	ppm TDS	bar	bar	kW	kW	kW	kWh/m3	%
PFD-Internal-PCR	7.25	0	0.00	7.25	3.99	3.26	3.99	45.0	20.0	0.200	0.200	25.7	7.13	0.60	1.92	0.00	1.92	0.587	0
PFD-Internal-PCR	7.25	0	0.00	7.25	3.99	3.26	3.99	45.0	20.0	0.200	0.364	25.7	7.1	0.60	1.92	0.00	1.92	0.587	45.0
PFD-Internal-PCR	7.25	5	0.20	7.45	4.10	3.35	3.90	45.0	20.6	0.205	0.372	25.6	7.3	0.63	1.97	0.00	1.97	0.588	46.2
PFD-Internal-PCR	7.25	10	0.40	7.65	4.21	3.44	3.81	45.0	21.1	0.209	0.381	25.5	7.5	0.66	2.02	0.01	2.03	0.589	47.5
PFD-Internal-PCR	7.25	15	0.60	7.85	4.32	3.53	3.72	45.0	21.7	0.214	0.390	25.4	7.7	0.69	2.07	0.02	2.09	0.591	48.7
PFD-Internal-PCR	7.25	20	0.80	8.05	4.43	3.62	3.63	45.0	22.2	0.220	0.400	25.4	7.9	0.72	2.13	0.02	2.15	0.592	50.0
PFD-Internal-PCR	7.25	25	1.00	8.25	4.54	3.71	3.54	45.0	22.8	0.225	0.410	25.4	8.1	0.75	2.18	0.03	2.21	0.595	51.2
PFD-Internal-PCR	7.25	30	1.20	8.45	4.65	3.80	3.45	45.0	23.3	0.231	0.420	25.5	8.3	0.78	2.24	0.03	2.27	0.597	52.4
PFD-Internal-PCR	7.25	35	1.40	8.65	4.76	3.89	3.36	45.0	23.9	0.237	0.432	25.5	8.5	0.81	2.29	0.04	2.34	0.600	53.7
PFD-Internal-PCR	7.25	40	1.60	8.85	4.87	3.98	3.27	45.0	24.4	0.244	0.443	25.7	8.8	0.84	2.35	0.05	2.40	0.603	54.9
PFD-Internal-PCR	7.25	45	1.80	9.05	4.98	4.07	3.18	45.0	25.0	0.251	0.456	25.8	9.0	0.88	2.41	0.06	2.47	0.607	56.1
PFD-Internal-PCR	7.25	50	2.00	9.25	5.09	4.16	3.09	45.0	25.5	0.258	0.469	26.0	9.2	0.91	2.47	0.07	2.54	0.611	57.4
PFD-Internal-PCR	7.25	55	2.19	9.45	5.20	4.25	3.00	45.0	26.1	0.266	0.483	26.2	9.4	0.94	2.54	0.08	2.61	0.615	58.6
1B	2B	3B	4B	5B	6B	7B	8B	9B	10B	11B	12B	13B	14B	15B	16B	17B	18B	19B	20B

(C) EXTERNAL PFD-PCR SIMULATION

	Module flow rates and flux									Module Concentrations			Pressure, power and energy						system
	HP	PCR		inlet	outlet	Perm.	Brine	MR	Flux	Inlet	outlet	Perm	p_{ap} (HP)	Δp(CP)	HP	CP	HP+CP	SE	REC
MODE	m3h	%	m3/h	m3/h	m3h	m3h	m3h	%	lmh	%	%	ppm TDS	bar	bar	kW	kW	kW	kWh/m3	%
PFD External PCR	7.25	0	0.00	7.25	3.99	3.26	3.99	45.0	20.0	0.200	0.200	25.7	7.1	0.60	1.92	0.00	1.92	0.587	0
PFD External PCR	7.25	0	0.00	7.25	3.99	3.26	3.99	45.0	20.0	0.200	0.364	25.7	7.1	0.60	1.92	0.00	1.92	0.587	45.0
PFD External PCR	7.25	5	0.20	7.25	3.99	3.26	3.99	45.0	20.0	0.205	0.372	26.3	7.2	0.60	1.93	0.00	1.94	0.594	46.3
PFD External PCR	7.25	10	0.40	7.25	3.99	3.26	3.99	45.0	20.0	0.210	0.382	26.9	7.3	0.60	1.95	0.01	1.96	0.601	47.6
PFD External PCR	7.25	15	0.60	7.25	3.99	3.26	3.99	45.0	20.0	0.216	0.393	27.7	7.4	0.60	1.98	0.01	1.99	0.610	49.0
PFD External PCR	7.25	20	0.80	7.25	3.99	3.26	3.99	45.0	20.0	0.223	0.405	28.6	7.5	0.60	2.00	0.02	2.02	0.619	50.6
PFD External PCR	7.25	25	1.00	7.25	3.99	3.26	3.99	45.0	20.0	0.230	0.418	29.5	7.6	0.60	2.03	0.02	2.05	0.629	52.2
PFD External PCR	7.25	30	1.20	7.25	3.99	3.26	3.99	45.0	20.0	0.239	0.434	30.6	7.7	0.60	2.06	0.03	2.09	0.640	53.9
PFD External PCR	7.25	35	1.40	7.25	3.99	3.26	3.99	45.0	20.0	0.248	0.452	31.9	7.8	0.60	2.10	0.03	2.13	0.653	55.7
PFD External PCR	7.25	40	1.60	7.25	3.99	3.26	3.99	45.0	20.0	0.260	0.473	33.4	8.0	0.60	2.14	0.04	2.18	0.668	57.7
PFD External PCR	7.25	45	1.80	7.25	3.99	3.26	3.99	45.0	20.0	0.274	0.498	35.1	8.2	0.60	2.20	0.04	2.24	0.685	59.8
PFD External PCR	7.25	50	2.00	7.25	3.99	3.26	3.99	45.0	20.0	0.290	0.527	37.2	8.4	0.60	2.26	0.04	2.30	0.705	62.1
PFD External PCR	7.25	55	2.19	7.25	3.99	3.26	3.99	45.0	20.0	0.310	0.564	39.8	8.7	0.60	2.33	0.05	2.38	0.730	64.5
1C	2C	3C	4C	5C	6C	7C	8C	9C	10C	11C	12C	13C	14C	15C	16C	17C	18C	19C	20C

average concentration polarization factor (*pf*, 1.25). Modules flow rates (inlet, outlet, and permeate) of the CCD and PFD of 0% PCR processes are the same, remain unchanged for CCD and external-PCR PFD, and vary for internal-PCR PFD as function of % PCR. Recovery increase for CCD is a function of batch progression irrespective of MR and flux; increased flux concomitant with % PCR of unchanged MR for internal-PCR PFD; and increased flow ratio of recycled brine at inlet to the HP pump for external-PCR PFD. Although CCD and internal/external PCR PFD are different processes, a meaningful comparison between them in terms of recovery, energy consumption, and quality of permeates is made possible when such processes are operated with the same MR, AEC, and av-*pf* and such an approach is exemplified in Table 1(A)–(C) for the desalination of 0.2% NaCl feed with unchanged MR (45%), AEC (13.9%) and av-*pf* (1.25) of same initial module flow rates and flux.

Simulated CCD data in Table 1(A), identified by a column label at the bottom, include the CCD cycle number (**2A**); module inlet (**3A**) and outlet (**4A**) concentrations; cycle duration (**5A**); applied pressure (**6A**); average applied pressure (**7A**); power of HP (**8A**), CP (**9A**) and HP+CP combined (**10A**); average specific energy (SE) per cycle (**11A**); av-TDS of permeates per cycle (**12A**); cumulative sequential time (**13A**); permeate volume production per cycle (**14A**); cumulative permeate volume production during the batch sequence progression (**15A**); cumulative energy consumption during the batch sequence progression (**16A**); batch sequence recovery (**17A**); av-SE (**18A**); and av-TDS of permeates (**19A**). Simulated PFD data for the internal (Table 1(B)) and external (Table 1(C)) PCR processes includes flow rates of HP (**2B** and **2C**); PCR (**4B** and **4C**), module inlet (**5B** and **5C**), module outlet (**6B** and **6C**), permeate (**7B** and 7**C**), and brine (**8B** and **8C**) with % PCR, MR, and flux revealed in columns **3B** and **3C**, **9B** and **9C,** and **10B** and **10C**, respectively. PDF recovery of internal-PCR (**20B**) is derived from the flow rates of HP and permeates, while that for external-PCR (**20C**) from the flow rate difference of HP less PCR and permeates. Module outlet concentrations (**12B** and **12C**) in the PCR–PFD processes are derived from the initial feed concentration and the recovery terms, while inlet module concentrations (**11B** and **11C**) are derived from the outlet concentrations and the MR terms. Permeates TDS (**13B** and **13C**) are derived from the salt diffusion coefficient of the element and flux accounting for the TCF. Applied pressures of HP (**14B** and **14C**) are derived from the permeability coefficient of the element, flux, average concentrate-side osmotic pressures of module, and pressure-difference (Δp) along pressure vessels (**15B** and **15C**) and derived from the module inlet-outlet average flow rate and the element-number per module. The power terms of HP (**16BC**), CP (**17BC**), and HP + CP (**18BC**) are derived by conventional pressure-flow power equations accounting for the efficiency factor of pumps, and the SE terms (**19B** and **19C**) are derived from power divided by permeate flow rate expressions. The cited term "derived" implies calculated by means of the appropriate conventional RO equation [1]. Identical parameters in Table 1(A)–(C) are calculated by means of the same equations in order to maintain uniformity of data of trustworthy relationships not influence by different computation techniques.

The comparative results according to the data in Table 1(A) and 1(B) for the CCD and PFD–PCR ME4 (E = ESPA2-MAX) apparatus under review (Fig. 1(B)–(D)) with 0.20% NaCl at 45% MR are displayed on the recovery scale for module inlet and outlet concentrations in Fig. 2 as well as on the recovery (A) and PCR (B) scales in Fig. 3(A) and 3(B) for flow rates; in Fig. 4(A) and 4(B) for flux and MR; in Fig. 5(A) and 5(B) for module pressure-difference (Δp) and average concentration polarization; in Fig. 6(A) and 6(B) for applied pressure; in Fig. 7(A) and 7(B) for specific energy; in Fig. 8(A) and 8(B) for entropy efficiency; and in Fig. 9(A) and 9(B) for TDS of permeates. It should be pointed out the figures pertaining to the PCR scale (B) are only for the PFD–PCR processes, since no PCR takes place during CCD.

4. Comparative CCD and PFD–PCR theoretical model performance of ME4 (E = ESPA2-MAX) with 0.2% NaCl as function of MR, PCR, and recovery

The theoretical model database in Table 1(A)–(C) enables us to analyze the performance of the different CCD and PFD–PCR types of processes as function of MR, PCR, and recovery either separately or comparatively, and the results of such a study are presented next. MR selection in the database displayed in Table 1(A)–(C) of 35% (10.2% AEF, 1.18 av-*pf*); 40% (12.0% AEF, 1.21 av-*pf*); 45% (13.9% AEF, 1.25 av-*pf*); and 50% (15.9% AEF, 1.29 av-*pf)* gave complete set of results per each MR of the comparative pertinent results displayed in Figs. 10–13 as follows: The CCD comparative dependence on recovery and MR of SE is described in Fig. 10(A) and of TDS of permeates in Fig. 10(B). The PFD comparative dependence of SE on MR and PCR is described in Fig. 11(A) and on MR and recovery in Fig. 11(B). The PFD comparative dependence of TDS of permeates on MR and PCR is described in Fig. 12(A) and on MR and recovery in Fig. 12(B). The relationships between recovery and PCR in the PFD processes under review are displayed in Fig. 13.

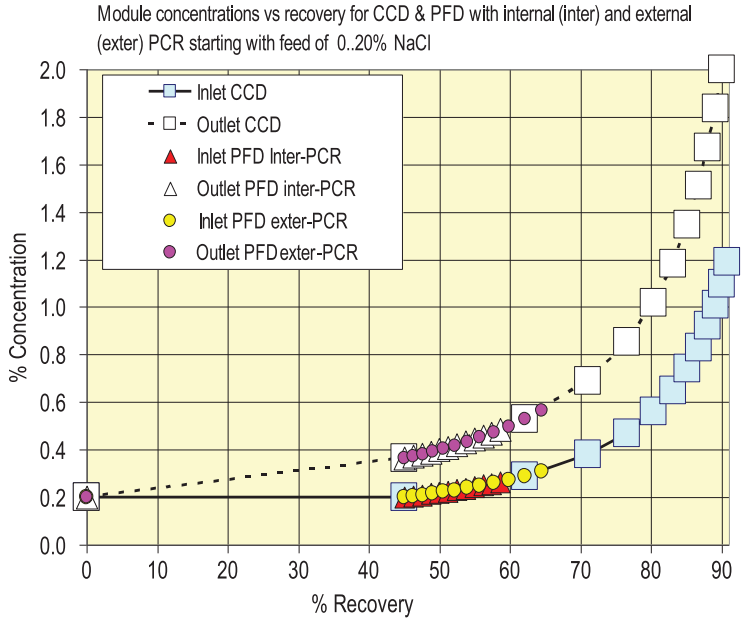

Fig. 2. Concentrations vs. recovery in the compared CCD and PFD–PCR ME4 (E = ESPA2-MAX) apparatus (Fig. 1(B)–(D)) at 45% MR with 0.2% NaCl feed according to the data in Table 1(A)–(C).

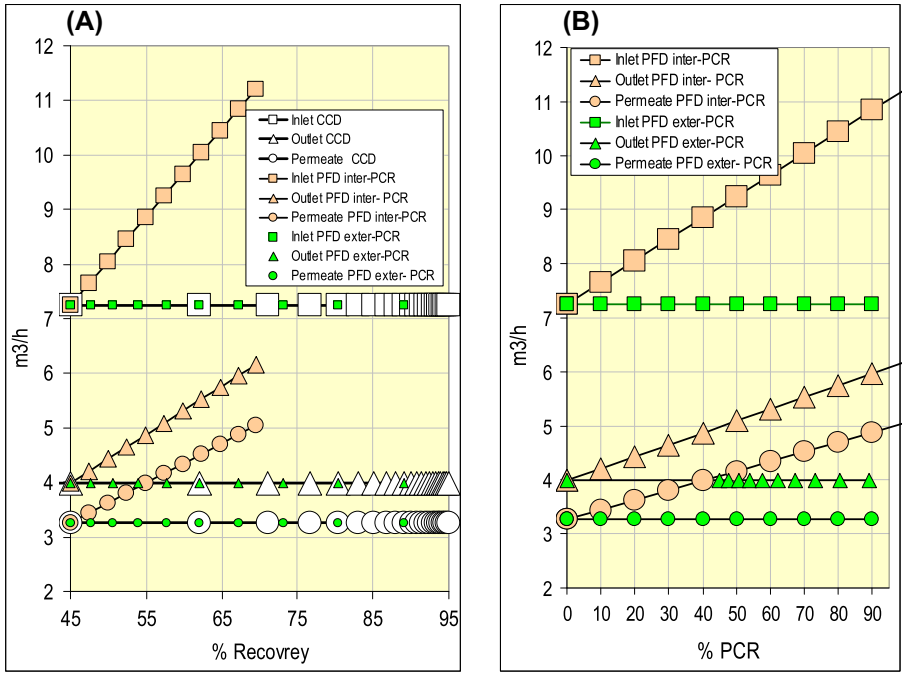

Fig. 3. Flow rates as a function of recovery (A) and PCR (B) in the compared CCD and PFD–PCR ME4 (E = ESPA2-MAX) apparatus (Fig. 1(B)–(D)) at 45% MR with 0.2% NaCl feed according to the data in Table 1(A)–(C)—The PCR scale figure (B) pertains only to PFD–PCR processes, since PCR doesn't take place during CCD.

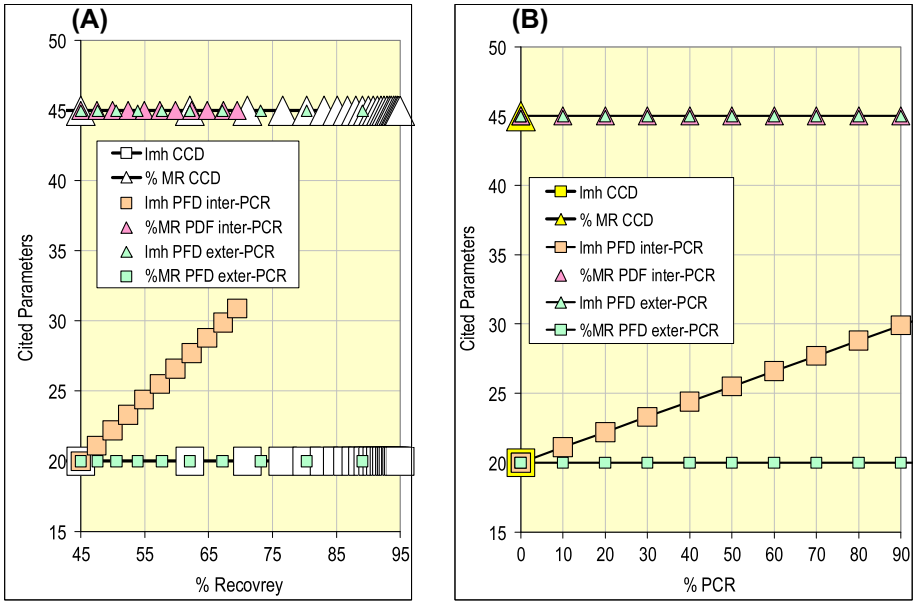

Fig. 4. Flux and MR as a function of recovery (A) and PCR (B) in the compared CCD and PFD–PCR ME4 (E = ESPA2-MAX) apparatus (Fig. 1(B)–(D)) at 45% MR with 0.2% NaCl feed according to the data in Table 1(A)–(C)—The PCR scale figure (B) pertains only to PFD–PCR processes, since PCR doesn't take place during CCD.

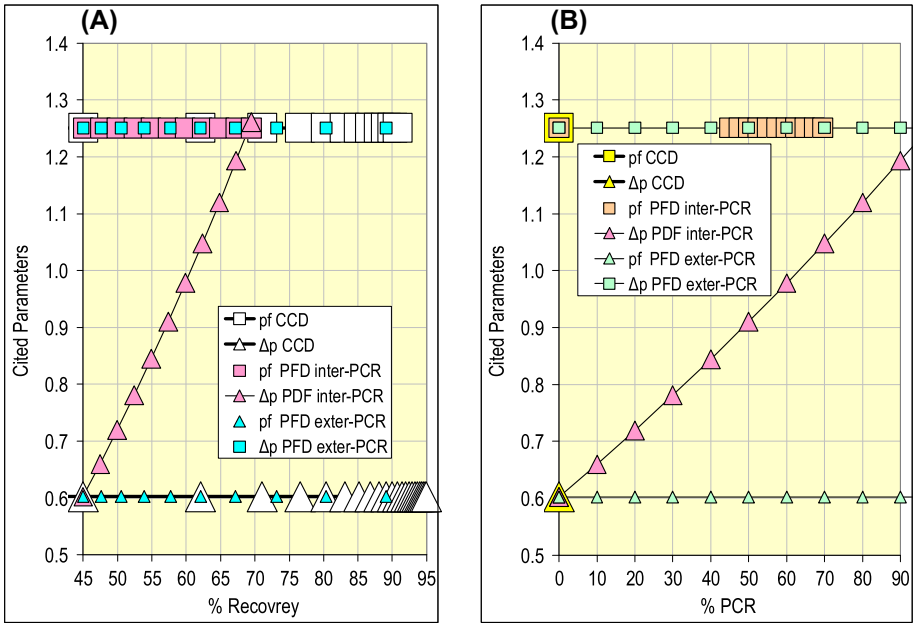

Fig. 5. Module pressure-difference (Δp) and average concentration polarization (av-pf) as a function of recovery (A) and PCR (B) in the compared CCD and PFD–PCR ME4 (E = ESPA2-MAX) apparatus (Fig. 1(B)–(D)) at 45% MR with 0.2% NaCl feed according to the data in Table 1(A)–(C)—The PCR scale figure (B) pertains only to PFD–PCR processes, since PCR doesn't take place during CCD.

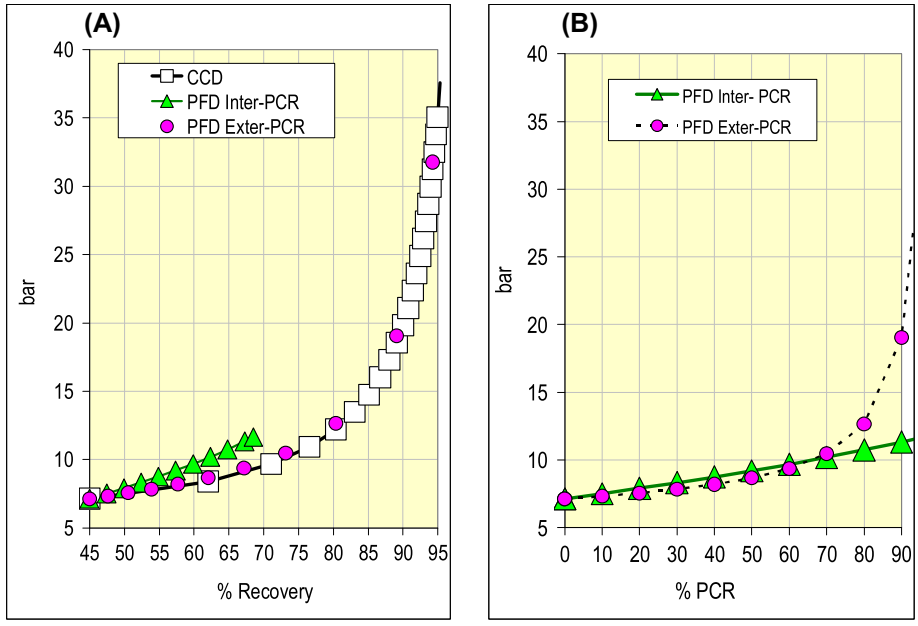

Fig. 6. Applied pressure as a function of recovery (A) and PCR (B) in the compared CCD and PFD–PCR ME4 (E = ESPA2-MAX) apparatus (Fig. 1(B)–(D)) at 45% MR with 0.2% NaCl feed according to the data in Table 1(A)–(C)—The PCR scale figure (B) pertains only to PFD–PCR processes, since PCR doesn't take place during CCD.

5. Discussion

The purpose of this study is to compare between three different BWRO technologies, two of which implicate partial recycling of concentrates referred to as PFD–PCR and batch CCD of complete concentrates recycling of the designs revealed in Fig. 1(B) and 1(D). In case of PFD–PCR processes distinction is made between internal recycling according to the design in Fig. 1(B) and external recycling according to the design in Fig. 1(C). Parameters selection in the simulations under review covers noteworthy features such as 0.2 NaCl feed salinity typical of common brackish water sources in the EC range of 2,500–3,700 μS/cm; four-element module designs (Fig. 1(A) and 1(D)) in the context of the MR range 35% (10.2% AEF, 1.18 av-*pf*)–50% (15.9% AEF, 1.29 av-*pf)* which manifest the effective productivity range of the front elements in conventional BWRO modules at flux of 20 lmh or higher without exceeding the elements' performance specifications recommended by their manufacturers; and a wide range PCR of 0–99% for the PFD processes with zero PCR corresponding to the module design (Fig. 1(A)) where PCR is not possible. In simple terms, the simulated data pertain to all the four structural designs depicted in Fig. 1(A)–(D) under ordinary performance conditions with common feed sources without exceeding specifications of elements.

The model simulation performance at 45% MR, illustrated in Figs. 2–9, provides a rather comprehensive comparative data for the processes under view from the stand-points of recovery and PCR. Module inlet and outlet concentrations as function of recovery displayed in Fig. 2 are the same for the different processes in accordance with theory. Module flow rates as function of recovery (Fig. 3(A)) and PCR (Fig. 2(B)) at 45% MR reveal identical flow rates for all three processes at start, and thereafter, increased flow rates only for the internal PCR–PFD process as function PCR. All three processes proceed with an identical MR of 45% (Fig. 4(A) and 4(B)) and av-*pf* 1.25 (Fig. 5(A) and 5(B)) and the internal and external PCR processes are distinguished from each other by increased flux (Fig. 4(A) and 4(B)) and Δp (Fig. 5(A) and 5(B)) only in case of internal-PCR. The internal PCR–PFD process is also distinguished from the others by the limited raise of recovery with PCR in the range of 45–70%. Dependence of applied pressure on recovery (Fig. 6(A)) and PCR (Fig. 6(B)) for the PFD processes under review manifests an increased pressure demand for the internal PCR process as expected due to increased flux; whereas, both the external PCR and CCD processes of the same operational flux also show identical applied pressure requirements. Energy aspects displayed in Fig. 7(A) and 7(B) reveal the clear advantage of CCD over PFD–PCR in the entire recovery range (0–95%) and the inferior results for PFD with external PCR in particular where energy rise with PCR is exponential and fast (Fig. 7(B)). Entropy efficiency (EE) of the compared processes (Fig. 8(A) and 8(B)) manifests

the mirror image of the SE results and reveals much higher efficiency of the CCD process which proceeds with near absolute energy conversion efficiency without waste of brine energy losses. The EE benefit of CCD over PFD–PCR is maintained even at high recovery where the brine energy losses of the compared PFD–PCR processes become small. The greater decline in EE with recovery and PCR observed for external PCR compared with internal PCR (Fig. 8(A) and 8(B)) manifests greater entropy losses to the environment with declined reversibility for the former process. Permeates' TDS in the compared processes displayed in Fig. 9(A) and 9(B) reveals similar results for CCD and internal PCR–PFD and inferior quality permeates for external PCR–PFD with increased recovery and/or PCR. Summary of results for the compared processes of fixed MR (45%) with identical modules' flow rates at start of 20 lmh permeation reveals the following noteworthy features:

(1) CCD-batch: A process of the lowest energy and highest recovery amongst the compared processes with TDS of permeates being only slightly inferior to those of the internal PCR–PFD process.
(2) Internal PCR–PFD: A process of a much higher energy demand compared with CCD, a small energy rise as function of PCR, a recovery range confined to 70% at 90% PCR, and low TDS of permeates just below the value of CCD.
(3) External PCR–PFD: A process of the highest energy and TDS of permeates amongst the compared processes of high recovery as function of a fast exponential rise with PCR.

The results of the extended comparative study which also takes account of MR variations are provided separately for CCD (Fig. 10(A) and 10(B)) and for the PFD–PCR processes (Figs. 10–13), since the former proceeds without PCR. MR effects on CCD in the model system under review according to the MR-adjusted database in Table 1(A) and 1(C) are displayed for SE in Fig. 10(A) and for TDS of permeates in Fig. 10(B) and the results in these figures reveal small differences at start of the batch processes of a declined energy gap with MR rise, and an opposite effect of declined TDS with MR drop. Maximum separation between curves in Fig. 10(A) and 10(B) is noticed in the initial CCD cycle, declines thereafter, and all curves ultimately merge above 80% recovery. The average MR effect on energy and TDS of permeates as function of recovery is manifested in the system under review by the average MR value (42.5%).

Energy consumption as function of PCR for the PDF processes under review (Fig. 11(A)) reveals a trend of increased consumption with declined MR

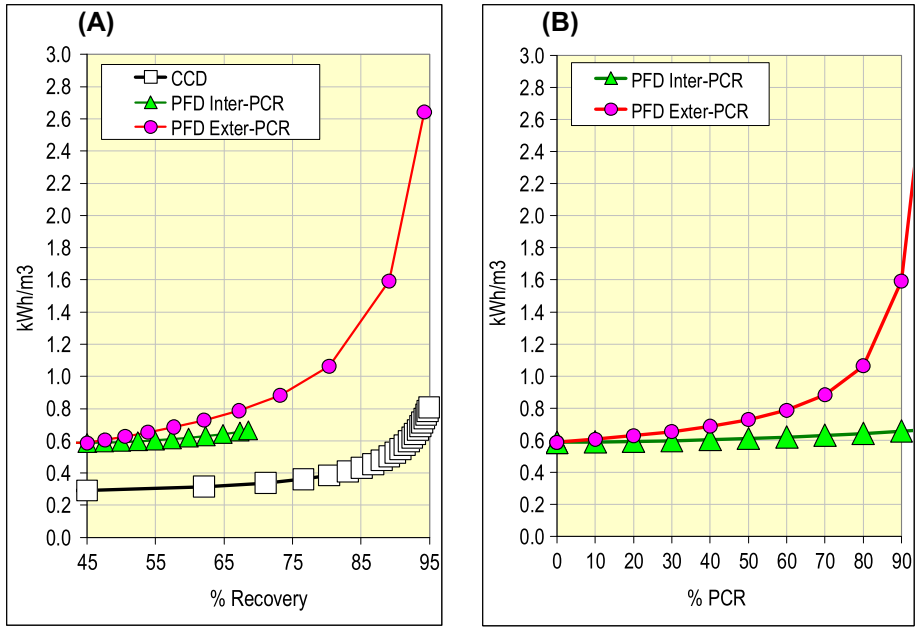

Fig. 7. Specific energy (SE) as a function of recovery (A) and PCR (B) in the compared CCD and PFD–PCR ME4 (E = ESPA2-MAX) apparatus (Fig. 1(B)–(D)) at 45% MR with 0.2% NaCl feed according to the data in Table 1(A)–(C)—The PCR scale figure (B) pertains only to PFD–PCR processes, since PCR doesn't take place during CCD.

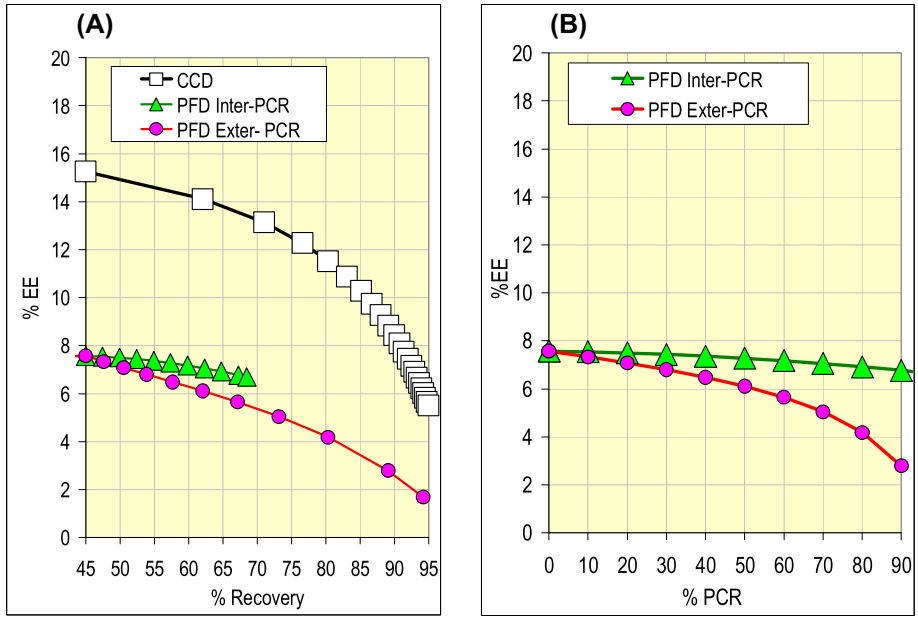

Fig. 8. Entropy efficiency (EE) as function of recovery (A) and PCR (B) in the compared CCD and PFD–PCR ME4 (E = ESPA2-MAX) apparatus (Fig. 1(B)–(D)) at 45% MR with 0.2% NaCl feed according to the data in Table 1(A)–(C)—EE stands for the ratio of the least minimum SE under infinitesimal flux (1.6 bar atm or 0.0444 kWh/m^3) and the simulated SE in the system under review—The PCR scale figure (B) pertains only to PFD–PCR processes, since PCR doesn't take place during CCD.

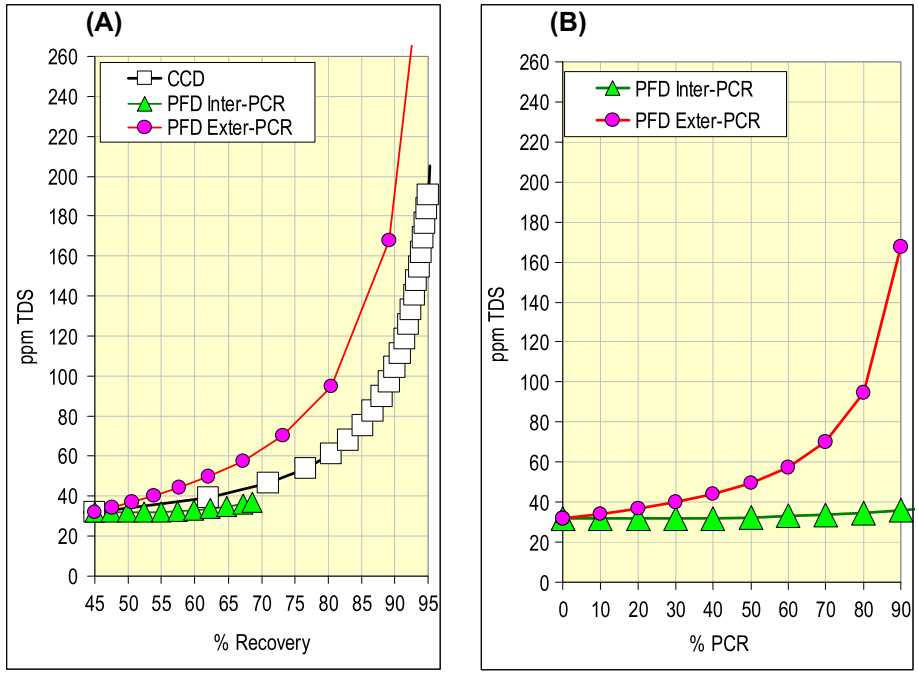

Fig. 9. Permeates' TDS as a function of recovery (A) and PCR (B) in the compared CCD and PFD–PCR ME4 (E = ESPA2-MAX) apparatus (Fig. 1(B)–(D)) at 45% MR with 0.2% NaCl feed according to the data in Table 1(A)–(C)—The PCR scale figure (B) pertains only to PFD–PCR processes, since PCR doesn't take place during CCD.

(maximum at 35% MR); however, this trend for internal-PCR is linear and small, whereas that for external-PCR is exponential and large. Energy consumption as function of recovery for the PDF processes under review (Fig. 11(B)) reveals the same above-cited trends of increased consumption with declined MR, and the reference to the average CCD energy displayed in Fig. 11(B) provides illustrates the enormous energy-saving prospects of CCD including at high recovery. Noteworthy in Fig. 11(B) is the fine structure of the internal PCD–PFD process which shows increased recovery with MR (parenthesis) in the approximate order 60% (35% MR); 65% (40% MR); 70% (45% MR); and 75% (50% MR). The MR effects on the TDS of permeates for the PDF processes under review as function of PCR (Fig. 12(A)) reveal small near linear variations for the internal PCR–PFD process of increased quality (lower TDS) with declined MR and large exponential variations in the same order for the external PCR process. The MR effect on the TDS of permeates for the PDF processes under review on the recovery scale (Fig. 12(B)), appear to be rather small and of the same pattern revealed on the PCR scale (Fig. 12(A)).

Since the primary intent of PCR is to increase the recovery of a conventional PFD system, noteworthy in the context of the present study is the relationships between recovery and PCR as function of MR in Fig. 13 for four-element single module designs (Fig. 1(A)–(D)) according to MR-adjusted database in Table 1(A)–(C). For internal PCD–PFD in the context of the investigated model, the figure shows linear relationships between recovery and PCD with increased recovery associated with greater MR. In addition, the figure also shows the recovery limits for internal PCR–PFD, with maximum recovery of 70% for the design under review attained with 50% MR and 100% PCR. In the case of external PCR–PFD processes, the overall pattern is the same; however, the relationships are non-linear of increased exponential nature with recovery. The comparative model simulation results of the processes under review in Figs. 10–13 reveal that CCD is the best process by far to achieve high recovery with exceptionally low energy, unmatched by conventional PFD methods including such with either internal or external PCR. While PFD with internal-PCR gave permeates of somewhat better quality compared with CCD, increase recovery with PCR by this technique is limited and proceed with a much greater energy demand. While PFD with external-PCR allows increased recovery comparable to that of CCD, this is achieved at an expense of inferior quality permeates

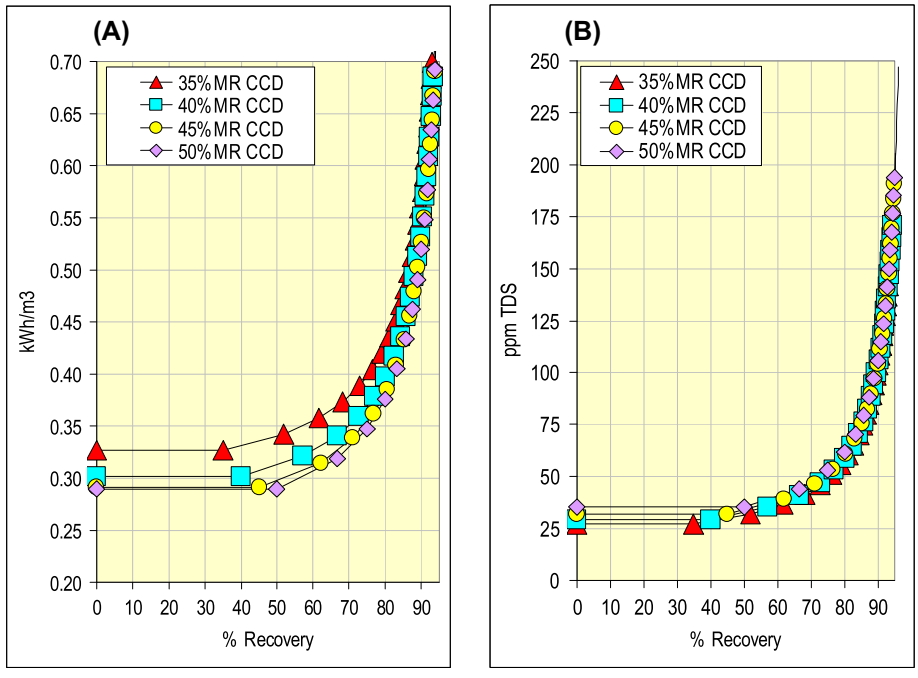

Fig. 10. Specific energy (A) and permeates' TDS (B) as a function of recovery and MR for the CCD ME4 (E = ESPA2-MAX) apparatus (Fig. 1(D)), generated by the adjusted simulation database in Table 1(A) for 0.2% NaCl and flux of 20 lmh.

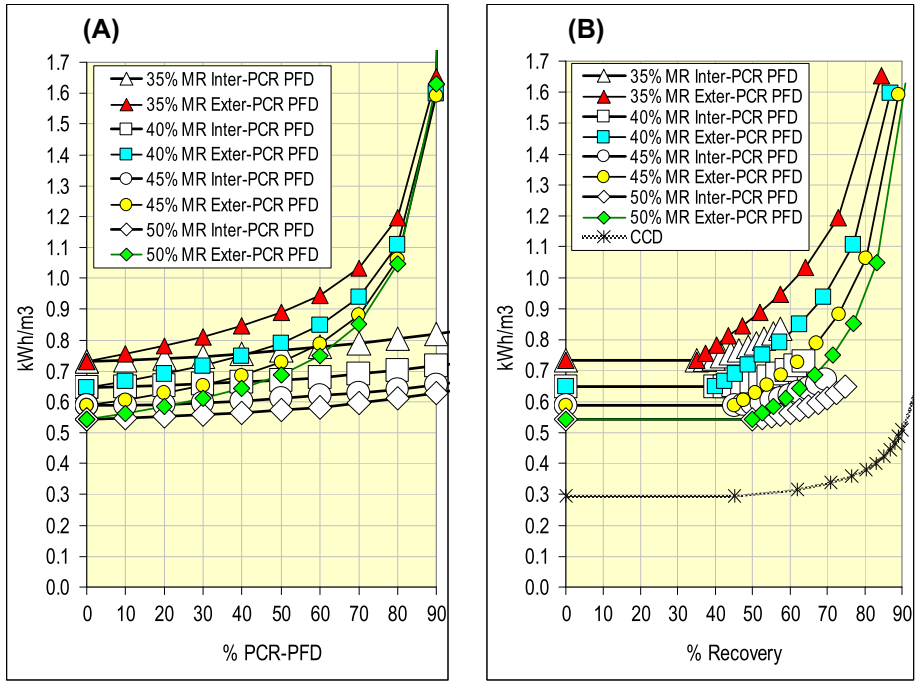

Fig. 11. Specific energy dependence on PCR (A) and recovery (B) as a function of MR for the PFD–PCR ME4 (E = ESPA2-MAX) apparatus (Fig. 1(B) and 1(C)), generated by the adjusted simulation database in Table 1(B) and 1(C) for 0.20% NaCl feed—The SE CCD line in (B) is the average of Fig. 10(A).

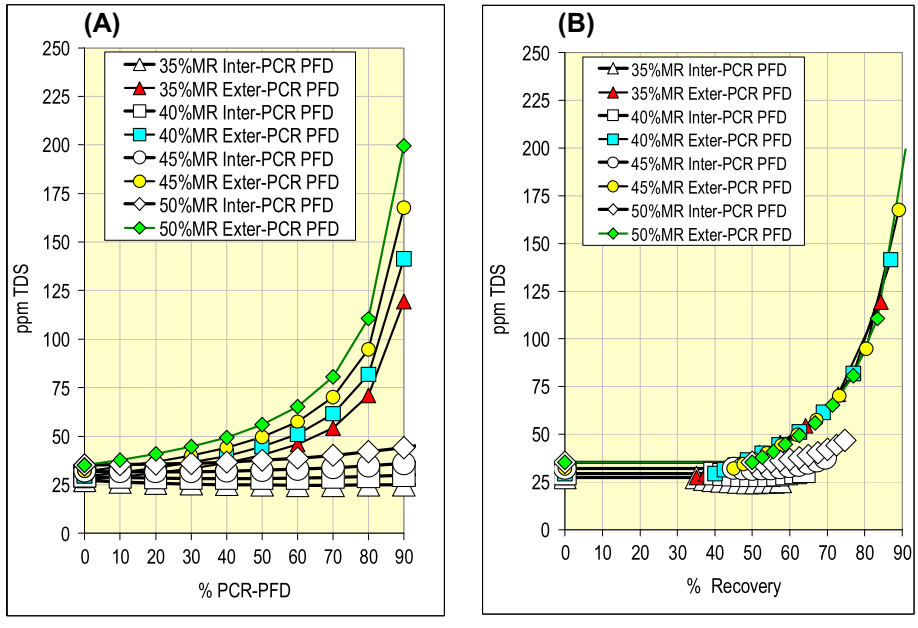

Fig. 12. Permeates' TDS dependence on PCR (A) and recovery (B) as a function of MR for the PFD–PCR ME4 (E = ESPA2-MAX) apparatus (Fig. 1(B) and 1(C)), generated by the simulation data base in Table 1(B) and 1(C) A for 0.2% NaCl feed.

and exceptionally high energy consumption. The trends revealed in the model study under review are of general implications and should apply to non-staged BWRO designs like Fig. 1(A)–(D) with multiple modules arranged in parallel of selected number of elements per module, as well as to BWRO staged system designs with PCR means. CCD can be operated under fixed flow and variable pressure conditions or

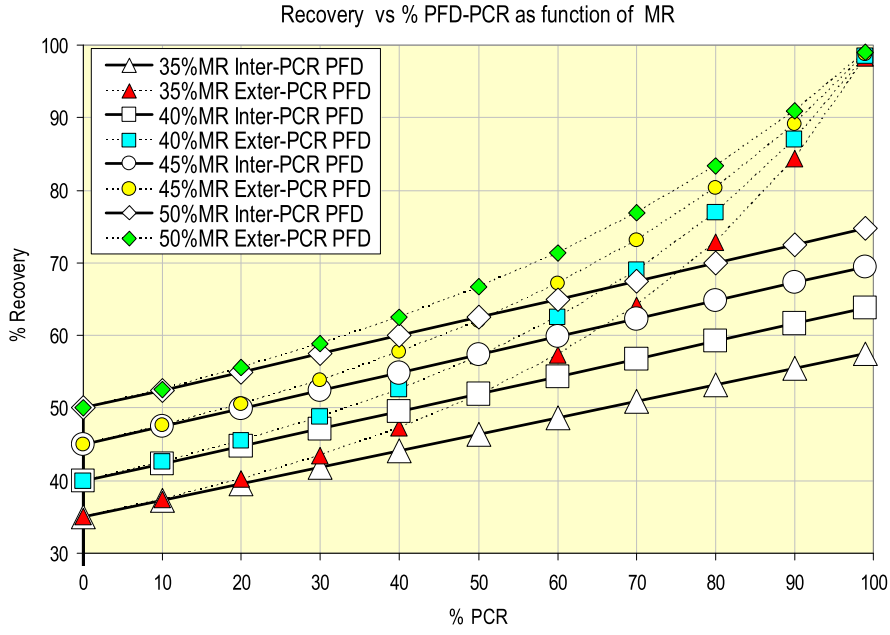

Fig. 13. Recovery vs. PCR as a function of MR for the PFD–PCR ME4 (E = ESPA2-MAX) apparatus (Fig. 1(B) and 1(C)), generated by the adjusted simulation database in Table 1(B) and 1(C) for 0.2% NaCl feed.

under fixed pressure and variable flow conditions [8] and therefore, it is pertinent to point out that only the former mode of operation is considered in the context of the present study.

Conventional two-stage PFD systems with six-element modules are generally designed for 75–80% recovery and three-stage systems for 85–90% recovery without exceeding the performance specifications of elements, and the recovery of such systems can be increased somewhat by the implication PCR and this at the expense of increased energy consumption and propensity for scaling and fouling. In contrast with PFD with or without PCR, batch-CCD operates on the basis of different principles with complete concentrate recycling and dilution with pressurized feed at module inlet under fixed flow and variable pressure conditions without any brine energy losses. Under the specified batch-CCD operational conditions, the process proceeds with near absolute energy conversion efficiency, low energy consumption manifested by the batch average, high recovery confined only by the constituents of the source, and low propensity for scaling and fouling due to the dilution effect at module inlet and controlled cross-flow independent of flux and/or recovery—features unattainable by conventional PFD techniques. Making batch CCD continued for commercial applications with retention of its unique operational features led to the development of consecutive sequential batch desalination techniques by the implication in the design of a side-conduit (e.g. Fig. 14) or by the incorporation in the process of a brief PFD step for brine replacement with feed between extended CCD sequences (e.g. Fig. 15). Retention of the batch-CCD properties with Fig. 14 like

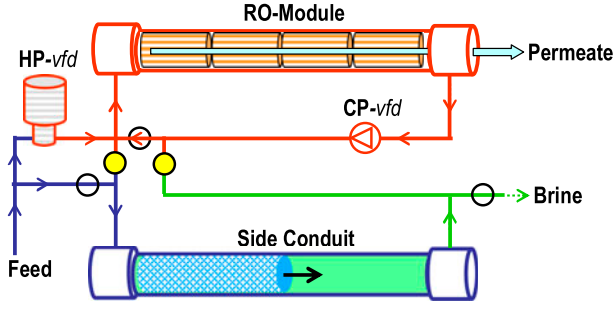

Fig. 14. Schematic illustration of a CCD-RO apparatus for continuous consecutive sequential batch desalination under fixed flow and variable pressure conditions of near absolute energy conversion efficiency without need for energy recovery device (ERD) comprising, a four-element module, a side-conduit (SC), a high pressure pump means with *vfd* (HP-*vfd*), circulation means with *vfd* (CP-*vfd*), and valve means (circles); showing a stage in the process where desalination is continued and the disengaged SC undergoing replacement of brine with fresh feed at near atmospheric pressure. Colors: red for pressurized section; blue and greed for non-pressurized sections with former for feed and latter for brine.

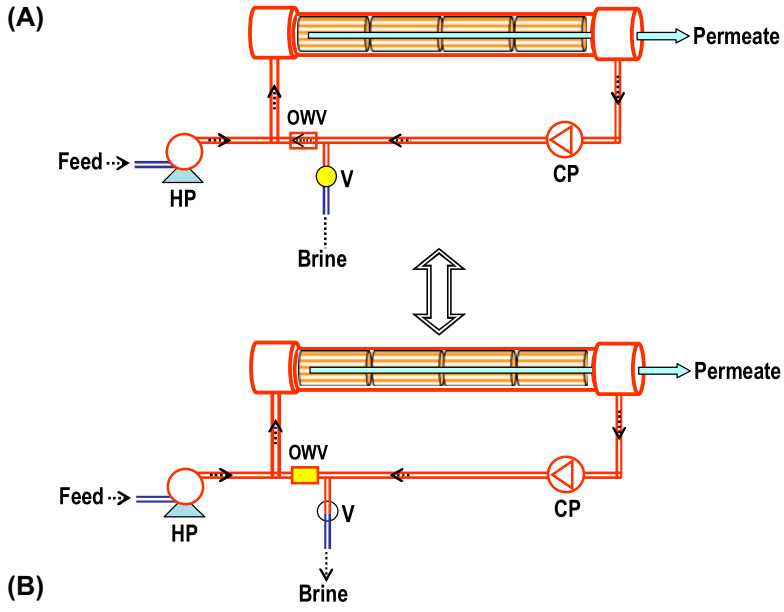

Fig. 15. Schematic design of a four-element module BWRO-CCD apparatus for a two-mode consecutive sequential batch desalination process involving CCD cycles under fixed flow and variable pressure conditions experienced most of the time and brief PFD steps between CCD sequences at the desired recovery for the replacement of brine by fresh feed without stopping desalination. (A) CCD experience most of the (>90%) with $Q_{HP} = Q_{PERM}$ and (B) PFD brief flush steps with $Q_{HP} = Q_{PERM} + Q_{BRINE}$ between CCD sequences.
Abbreviations: HP-*vfd*, high pressure pump with *vfd* means; CP, CP with *vfd* means; OWV, one way valve (check valve) means; and V, actuated valve means. Colors: red for pressurized section; blue for non-pressurized sections.

designs of multiple modules was reported for BWRO [13] and for SWRO [2–12] systems with record low energy (<1.7 kWh/m^3) demonstrated for 48% desalination of ocean seawater [11]. Noteworthy in particular are the reported results of 96% (0.34 kWh/m^3) desalination of domestic supplies (553 μS/cm) in Kansas City (USA) [21]; 93.8% (0.65 kWh/m^3) desalination of ground water (1,304 ppm TDS—57 ppm silica) in Fabbri farm (CA, USA) [22]; 93% desalination of treated domestic effluents by LA-Sanitation (CA, USA) [25]; 90% desalination of treated domestic effluents (1,300–1,800 μS/cm) in the Safdan-Center (Israel) [20], and other similar results. The aforementioned citations clearly supported the retention of the unique batch-CCD operational properties in the analogous consecutive-sequential batch desalination processes.

6. Concluding remarks and outlook

Deterioration/depletion of ground/surface freshwater supplies as a result of the expanding world population, increased standard of living, adverse environmental problems, and climate changes inflicted by enhancement of the global "greenhouse effect," led to urgent needs for advanced technologies for clean energy generation, recycling of wastewater for reuse, and creation new freshwater supplements by SWRO and BWRO desalination. Accordingly, future targets of the desalination energy [24] emphasize high recovery low energy processes in order to save water and energy and minimize the expensive handling of brine effluents from inland desalination plants. High recovery RO is made possible by PFD with internal/external PCR techniques [1] as well as by CCD [2–23] and the present study explores the relationships between them in terms of recovery, energy consumption, and quality of permeates under identical MR and av-*pf* of same or similar modules' flow rates conditions. The results of this study reveal the clear superiority of batch-CCD processes under fixed flow and variable conditions over conventional PFD processes with internal/external PCR for high recovery low energy desalination, since the CCD technologies [2–23] meet all future goals of the desalination industry already. Reported studies [2–23] of consecutive sequential CCD processes demonstrated their close tie to batch-CCD and opened the door to advanced desalination of enormous future prospects. Apart from high recovery low energy prospects unattainable by conventional PFD techniques, CCD offers technologies of low fouling and scaling propensity since during the consecutive sequential

cycles concentrates are continuously diluted with fresh feed at inlet to modules, and thereby enable optimization of such processes to the highest recovery made possible by the constituents of the source. Moreover, after each CCD consecutive sequence the entire content of the system is flushed out and replace by fresh feed, thereby avoiding the accumulation of fouling elements in the system, and this in contrast with internal/external PFD processes where the level of concentrates in the system remains constantly high in the absence of a brine flush-out procedure. The ability to perform BWRO of low fouling and scaling propensity implies a lesser need for CIP procedures and therefore, savings of CIP expenses and loss of permeate production during said CIP procedures.

Acknowledgments

Funds to *Desalitech Ltd*. by AQUAGRO FUND L.P. (Israel) and by Liberation Capital LLC (USA) and Spring Creek Investments (USA) are gratefully acknowledged.

References

[1] Dow Liquid Separation, FILMTEC™ Reverse Osmosis Membranes, "Technical Manual" "System Design", 2011, pp. 72–102. Available from: <http://msdssearch.dow.com>.
[2] A. Efraty, R.N. Barak, Z. Gal, Closed circuit desalination—A new low energy high recovery technology without energy recovery, Desalin. Water Treat. 31 (2011) 95–101.
[3] A. Efraty, R.N. Barak, Z. Gal, Closed circuit desalination series no-2: New affordable technology for sea water desalination of low energy and high flux using short modules without need of energy recovery, Desalin. Water Treat. 42 (2012) 189–196.
[4] A. Efraty, Closed circuit desalination series no-6: Conventional RO compared with the conceptually different new closed circuit desalination technology, Desalin. Water Treat. 41 (2012) 279–295.
[5] A. Efraty, Closed circuit desalination series no. 8: Record saving of RO energy by SWRO-CCD without need of energy recovery, Desalin. Water Treat. 52 (2014) 5717–5730.
[6] A. Efraty, CCD Series No-11: Single module compact SWRO-CCD units of low energy and high recovery for seawater desalination including with solar panels and wind turbines, Desalin. Water Treat. 53 (2015) 1162–1176.
[7] A. Efraty, CCD series no-13: Illustrating low-energy SWRO-CCD of 60% recovery and BWRO-CCD of 92% recovery with single element modules without energy recovery means—A theoretical extreme case study, Desalin. Water Treat. 57 (2016) 9148–9165.
[8] A. Efraty, CCD Series No-14: SWRO-CCD under fixed-pressure and variable flow compared with fixed-flow and variable pressure conditions, Desalin. Water Treat. 56 (2015) 875–893.
[9] A. Efraty, CCD Series No-15: Simple design batch SWRO-CCD units of high recovery and low energy without ERD for wide range flux operation of high cost-effectiveness, Desalin. Water Treat. 57 (2016) 9166–9179.
[10] A. Efraty, CCD series no-16: Opened vs. closed circuit SWRO batch desalination for volume reduction of silica containing effluents under super-saturation conditions, Desalin. Water Treat. 57 (2016) 9569–9584.
[11] Z. Gal, A. Efraty, CCD series no. 18: Record low energy in closed-circuit desalination of ocean seawater with nanoH_2O elements without ERD, Desalin. Water Treat. 57 (2016) 9180–9189.
[12] A. Efraty, CCD Series No. 19: The lowest energy prospects for SWRO through single-element modules under plug-flow and closed-circuit desalination conditions, Desalin. Water Treat. (2016), doi: 10.1080/19443994.2015.1126409.
[13] A. Efraty, Closed circuit desalination series no-3: High recovery low energy desalination of brackish water by a new two-mode consecutive sequential method, Desalin. Water Treat. 42 (2012) 256–261.
[14] A. Efraty, Closed circuit desalination series no-4: High recovery low energy desalination of brackish water by a new single stage method without any loss of brine energy, Desalin. Water Treat. 42 (2012) 262–268.
[15] A. Efraty, J. Septon, Closed circuit desalination series no-5: High recovery, reduced fouling and low energy nitrate decontamination by a cost-effective BWRO-CCD method, Desalin. Water Treat. 49 (2012) 384–389.
[16] A. Efraty, Z. Gal, Closed circuit desalination series No 7: Retrofit design for improved performance of conventional BWRO system, Desalin. Water Treat. 41 (2012) 301–307.
[17] A. Efraty, Closed circuit desalination series no-9: Theoretical model assessment of the flexible BWRO-CCD technology for high recovery, low energy and reduced fouling applications, Desalin. Water Treat. 53 (2015) 1755–1779.
[18] A. Efraty, CCD Series No-10: Small compact BWRO-CCD units of high recovery, low energy and reduced fouling for supplied water upgrade to industry, irrigation, domestic and medical applications, Desalin. Water Treat. 53(5) (2015) 1145–1161.
[19] A. Efraty, Closed circuit desalination series no-12: The use of 4, 5 and 6 element modules with the BWRO-CCD technology for high recovery, low energy and reduced fouling applications, Desalin. Water Treat. 53 (2015) 1780–1804.
[20] J. Septon, A. Efraty, CCD series no-17: Application of the BWRO-CCD technology for high-recovery low-energy desalination of domestic effluents, Desalin. Water Treat. 57 (2016) 9585–9601.
[21] Z. Gal, J. Septon, A. Efraty, A.-M. Lee, CCD Series no-20: High flux low energy upgrade of municipal water supplies with 96% recovery for boiler-feed and related applications, Desalin. Water Treat. (2016), doi: 10.1080/19443994.2015.1126413.

[22] V. Sonera, J. Septon, A. Efraty, CCD Series no-21: Illustration of high recovery (93.8%) of a silica containing (57 ppm) source by a powerful technology of volume reduction prospects, Desalin. Water Treat. (2016), doi: 10.1080/19443994.2015.1126412.
[23] A. Efraty, CCD Series no-22: Recent advances in RO, FO and PRO and their hybrids applications for high recovery desalination of treated sewage effluents, Desalination (2016), doi: 10.1016/j.desal.2016.01.009.
[24] N. Voutchkov, Membrane seawater desalination—Overview and recent trends, IDA conference, November 2–3, Riverside, CA, 2010.
[25] B. Mansell, T. Nikonova, P. Ackman, B. Langpap, C. C. Tang, R. Tremblay, P. Friess, Evaluation of RO concentrate treatment and disposal options for the Santa Clarita Valley, 29th Annual WateReuse Symposium, Dallas, TX, September 7–10, 2014.